LEED structural analysis of Al(111)-K-($\sqrt{3} \times \sqrt{3}$)$R30°$: Identification of stable and metastable adsorption sites

C. Stampfl, M. Scheffler, and H. Over*
Fritz-Haber-Institut der Max-Planck-Gesellschaft, Faradayweg 4-6, D-14 195 Berlin (Dahlem), Germany

J. Burchhardt, M. Nielsen, and D. L. Adams
Institute of Physics, Aarhus University, DK-8000 Aarhus C, Denmark

W. Moritz
Institut für Kristallographie und Mineralogie, Universität München, D-80333 München, Germany
(Received 22 June 1993)

A detailed low energy electron diffraction analysis has been performed to investigate the adsorption of potassium on Al(111) at 90 K and at 300 K. At each temperature a ($\sqrt{3} \times \sqrt{3}$)$R30°$ structure is formed, however, the adsorbate positions are different. For adsorption at 90 K the adatoms occupy on-top sites and at 300 K they occupy substitutional sites, both geometries have hitherto been regarded as very unusual. An irreversible phase transition from the former to the latter stable structure occurs on warming to 300 K. The obtained interatomic distances and surface relaxations are discussed in terms of an interplay of the electrostatic repulsion between adatoms and substrate screening as well as coordination number. An approximate scheme for including the effect of anisotropic atomic motions under the influence of thermal excitation was applied. It is found that the R factors for the on-top site are significantly improved whereas no improvement is found for the substitutional site.

I. INTRODUCTION

Recent studies of the adsorption of alkali-metal atoms on metal surfaces have revealed interesting and surprizing results which show that these systems are more complex than hitherto believed. In the standard picture of alkali-metal adsorption it is expected that on close-packed surfaces the adsorbates occupy high-symmetry sites without reconstruction of the substrate.[1–4] However, recent reports[1,5–13] have shown that in many cases this expectation is not realized. In particular, several determinations of occupation of on-top sites have appeared in the literature[5–8] and recently a more dramatic exception to the notion of simple adsorption has been reported in the occupation of the substitutional site identified by surface-extended x-ray-absorption fine structure (SEXAFS) for Na adsorption on Al(111),[9] as well as by density-functional theory calculations,[9,11] and for K on Al(111) as reported in our earlier paper.[12] Other very recent and interesting results of alkali-metal/metal systems have appeared. Andersen *et al.*[13] using high-resolution core-level spectroscopy and Aminpirooz *et al.*[14] using SEXAFS, have found for $c(2 \times 2)$-Na/Al(001) ($\Theta = 0.5$) that the local environment of the Na atom is different at low temperature and at room temperature. [We define coverage $\Theta = 1$ as having the same number of atoms as an Al(111) plane.] For adsorption at low temperature, both experimental results are consistent with the Na atoms occupying the four-fold hollow site. Adsorption at room temperature, however, appears to involve the formation of a surface alloy. Furthermore, Andersen *et al.*[15] have presented a high-resolution core-level spectroscopy study of submonolayer adsorption of Na, K, Rb, and Cs on the Al(111) surface at low temperature and at room temperature. They found that at low coverages the alkali-metal atoms adsorb at defects while at higher coverages island formation occurs in many cases. They argue that all of the ordered structures formed at room temperature involve a disruption of the Al(111) surface. In relation to this latter point, Kerkar *et al.*[16] have found for $p(2 \times 2)$-Na/Al(111) (coverage $\Theta = 0.5$) that at least two distinct Na adsorption sites are involved and propose a model involving two reconstructed layers, each of stoichiometry $NaAl_2$. Interesting results of alkali-metal adsorption on noble metals have also been reported, for example, two-dimensional (2D) condensation of K on Cu(001)[17] and K on Ag(001)[18] identified on the basis of low-energy-electron-diffraction (LEED) observations and by using soft-x-ray photoemission, respectively, which show that in these cases the adsorbate-adsorbate interaction overcomes the electrostatic repulsion and the surface-corrugation potential and that the adsorbate-substrate charge transfer is insignificant. Further, as shown by Lamble *et al.*[19] for Cs/Ag(111) using SEXAFS, it was found that for increasing coverage ($\Theta =$ 0.15 to 0.30) the Cs-Ag bond length increases by about 0.3 Å, interpreted by them as reflecting a transition in the cesium bonding from predominantly ionic to more covalent at high coverage (we note that it is possible that this could also be due to a switching of adsites accompanied by a variation of the bondlength due to different coordination number). For alkali-metal adsorption on (110)

metal surfaces the situation is somewhat different; it is well known that for these surfaces substrate reconstruction is often created by alkali-metal adsorption.[20]

The present system of interest, $(\sqrt{3} \times \sqrt{3})R30°$-K/Al(111), has been studied by Andersen *et al.*,[13] using high-resolution core-level spectroscopy, at both low temperature (100 K) and at room temperature, where strong changes in the core-level spectra with change in temperature are observed. This is consistent with the present results, where the adsorption of potassium on Al(111) has been investigated by LEED for low temperature (90 K) and for room temperature. In each case a $(\sqrt{3}\times\sqrt{3})R30°$ structure is formed. The LEED analysis reveals that the adsorbate position for the two temperatures is different and somewhat unusual: for adsorption at low temperature the adatoms occupy on-top sites on a rumpled substrate and at room temperature a reconstruction of the substrate occurs such that the K atoms occupy surface substitutional sites. That is, an irreversible order-order transition occurs from the former, metastable structure to the latter stable structure upon warming to room temperature without change in the 2D unit cell.

In this paper we present a detailed description of the LEED analysis reported in our earlier paper[12] which has been extended to investigate the effect of using a different inner potential in the adsorbate layer to that in the substrate, and to investigate the possibility that anisotropic temperature effects are significant in relation to the adsorbate by using the recent concept of "split positions" as introduced by Over, Moritz, and Ertl.[21] For K in the on-top position a relatively large lateral motion is found that could correspond to a soft surface phonon mode.

II. EXPERIMENT

All the LEED intensity measurements were performed at 90 K. The $(\sqrt{3}\times\sqrt{3})R30°$ structures for room temperature and low temperature were formed respectively by saturation adsorption at 300 K and by adsorption (not to saturation) at 90 K. Rutherford back-scattering measurements have shown that the former structure is formed by adsorption of K atoms with coverage $\Theta = 1/3$.[22] Auger electron spectroscopy (AES) measurements in the present work indicated that the structure formed by adsorption at 90 K also corresponds to coverage $\Theta = 1/3$.

The measurements were carried out in an ultrahigh-vacuum system, with base pressure 3×10^{-11} torr. The Al(111) crystal was cleaned by cycles of Ar^+ ion bombardment at 1 keV and annealing to 500 °C. The main remaining contaminant after the cleaning process was C, with a coverage of about $\Theta = 0.01$ as estimated from AES measurements. K was deposited onto the crystal by evaporation from a SAES source.[23] The deposition was carried out in a few minutes and the residual-gas pressure during evaporation was typically 4×10^{-10} torr. AES measurements taken after deposition and after completion of a set of LEED measurements indicated that surface contamination (almost entirely C) was less than $\Theta = 0.05$. Sharp $(\sqrt{3} \times \sqrt{3})R30°$ LEED patterns with good contrast were obtained after deposition of K ($\Theta = 1/3$) at 90 K or at 300 K. At coverages less than $\Theta = 1/3$ the fractional-order spots were diffuse, giving no indication of island formation, but a detailed examination of beam profiles was not performed.

The LEED intensity measurements were made using a video-LEED system,[24] the basic components of which were a light-sensitive video camera with silicon-intensifier-target phototube, a "frame-grabber" adaptor for digitalization of video images of the LEED pattern on the fluorescent screen of a rear-view LEED optics, and a 12 bit a/d adaptor for programming the electron energy and for reading the electron energy and beam current. The two adaptors were installed in an IBM PC/AT computer. The intensity of a particular diffracted beam at a particular energy was measured by summing the pixel intensities in a window centered on the diffraction spot. The spot intensity was corrected for background as measured by summing pixel intensities in windows above and below the diffraction spot, and was normalized for the electron beam current and for the variation of the spot intensity with the spot's position on the fluorescent screen (Lambert's law). The intensities of an arbitrary number of beams could be measured simultaneously (to within the 40 ms digitalization time). Determination of the spot intensities was carried out in real time (about 0.5 s per energy). Acquisition of an image of the LEED pattern at a given energy was carried out in parallel with the processing of the image acquired at the previous energy. The algorithm for tracking the movement of the diffraction spots with energy was based on a calibration of the magnification of the optical system and frame grabber, and was completely robust.

The intensity measurements were carried out at normal incidence, which was set to within ±0.1° with respect to rotations about each of two axes, mutually orthogonal and orthogonal to the incident electron beam direction. This was achieved by minimizing the R factor for the comparison of intensity-energy $[I(E)]$ curves for (nominally) symmetry-equivalent beams as a function of the two rotation angles.

The main difficulty in our implementation of the video-LEED technique is the restricted dynamic range resulting from the eight-bit representation of pixel intensities in commercial frame grabbers. In practice the problem is accentuated by noise (~3% of the full video signal) due to the dark current in the video camera. To alleviate this problem, the measurements for the generally weaker fractional-order beams were carried out separately from the measurements for the substrate beams, at a larger gain setting of the video amplifier of the camera. As a further step, the measurements for each of the two sets were divided into two energy ranges, with two different settings of the video gain. The $I(E)$ curves shown in the present paper have been corrected for differences in the video gain and are therefore on the same (but arbitrary) intensity scale. In studies carried out after completion of the present work we have further improved the signal-to-noise ratio by programming the video amplifier to achieve near saturation intensity for the brightest LEED spot at each energy.[25]

For each of the $(\sqrt{3} \times \sqrt{3})R30°$-K structures, $I(E)$ curves were measured at normal incidence for a wide energy range 50–450 eV for 20 diffracted beams, which reduced to four symmetry-inequivalent integral-order and four symmetry-inequivalent fractional-order beams. The intensities of symmetry-equivalent beams were averaged.

Although the same LEED patterns at both temperatures were observed, from comparison of the *experimental* LEED intensity curves for the two structures, as shown in Fig. 1, it can be seen that the corresponding surface structures must be quite different. Furthermore, intensities measured after adsorption at 90 K and warming to 300 K are identical to those measured after adsorption at 300 K alone, indicating the occurrence of an irreversible, order-preserving phase transition.

III. LEED CALCULATION

The LEED intensity calculations were performed using the fully dynamical calculation scheme,[26] which includes the possibility of automatic, simultaneous refinement of the structural parameters, the real part of the complex electron self-energy, and the effective Debye temperature.[27] The program uses the "layer KKR" (Korringa-Kohn-Rostoker) approach together with the "layer-doubling method."[28] The R_{DE} factor, defined by Kleinle, Moritz, and Ertl,[29] was used to characterize the agreement between experiment and theory. This R factor requires only a rather small set of data points at discrete energies (hence "DE").

The scattering from Al and K atoms was described using ten phase shifts calculated from the muffin-tin band-structure potentials of Moruzzi, Janak, and Williams.[30] Atomic scattering matrices were averaged for the effects of thermal vibrations using a single Debye temperature for the Al substrate (Θ_{Al}) and a different Debye temperature for the adsorbed K atoms (Θ_K), which was taken as a variable in the analysis. The real and imaginary parts of the complex electron self-energy, $\Sigma = V_o + iV_{im}$, were taken to be energy independent. A constant value of V_{im}=4.0 eV was used and V_o was optimized. For Al(111) taking a constant value of V_o seems to be a good approximation, as can be seen from Fig. 2, where the calculated and experimental peak positions are well matched at low and high energies. This is consistent with the results of an investigation into the possible energy dependence of V_o and V_{im} by Nielsen and Adams.[31] In this study they allowed a linear variation with energy and concluded that in both cases the effect is insignificant. The surface potential barrier was assumed to be a refracting but nonreflecting step of height V_o. As mentioned in the introduction, extended calculations were also made where the inner-potential (i.e., the real part of the complex electron self-energy) for the adlayer was different to that of the Al substrate, and for the importance of anisotropic temperature effects using the approximation with split positions.[21] The results of these calculations are described in Secs. IV B and IV C and in Sec. V.

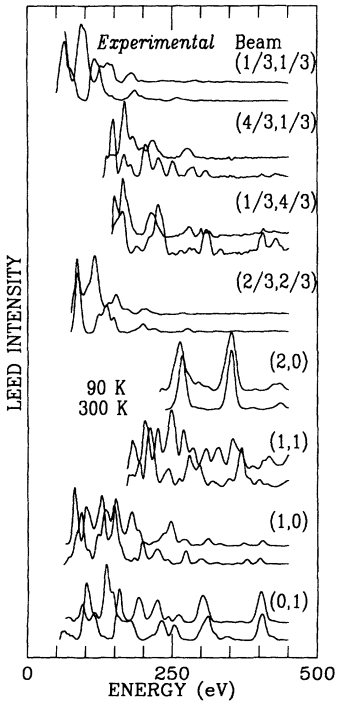

FIG. 1. Experimental intensity versus energy curves for the structures formed at room temperature and at low temperature. The upper and lower curves for each beam correspond to the low- and room- temperature results, respectively.

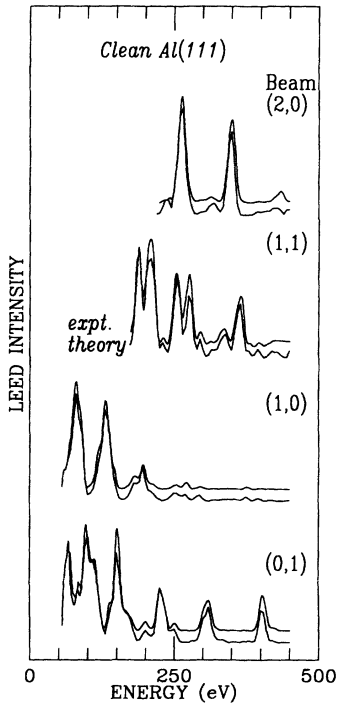

FIG. 2. Comparison of the experimental and theoretical LEED intensity curves for the clean Al(111) surface. The theoretical curves are the lower ones for each beam and the experimental results appear as the upper curve.

IV. RESULTS OF THE LEED ANALYSIS

A. The clean Al(111) surface

A structural analysis of the clean Al(111) surface was performed where it was found that the first aluminum interlayer spacing is expanded by 1.3 % ±0.8 % relative to the bulk interlayer spacing, in agreement with previous results in which expansions of 0.9 % ±0.5 % (Ref. 31) and 1.7 % ±0.3 % (Ref. 32) were found. The analysis, which was carried out for Θ_{Al} = 490 K (Ref. 31) and V_{im}=4.0 eV, led to an optimum value of $V_o = 6.0 \pm 1.0$ eV (with respect to the muffin-tin zero). The energy step used in the calculations was 5 eV, with four beams, which led to 234 data points being used in the comparison between theory and experiment. The R_{DE} factor was 0.193 and for the R factors of Pendry[33] and Zanazzi and Jona,[34] the values were R_P = 0.293 and R_{ZJ} = 0.121, respectively. As the LEED intensities were measured up to quite high energies, calculations were also performed using 14 phase shifts for Al, which led to slightly different R factor values (R_{DE} = 0.198, R_P = 0.235 and R_{ZJ} = 0.075) but no change in the determined structure. Figure 2 shows a comparison of the experimental curves and the calculated curves obtained for the clean Al(111) surface where good agreement can be seen.

B. The $(\sqrt{3} \times \sqrt{3})R30°$ structure: Low temperature

In the analysis of the LEED intensities, for each of the two $(\sqrt{3} \times \sqrt{3})R30°$ structures, five different adsorption sites were considered; namely, on-top, bridge, fcc and hcp hollow, and substitutional sites as shown in Fig. 3. In the first step of the analysis, the K-Al interlayer spacing (Z_K) and the first Al-Al interlayer spacing (D_{12}) were optimized, together with V_o. All other structural parameters were fixed at the ideal bulk values. In these calculations Θ_K was kept at 50 K and Θ_{Al} at 490 K. For this stage of the analysis the R_{DE} factor was used with an energy step of 10 eV.

For the structure formed at 90 K the initial analysis led to a rejection of the twofold bridge and threefold fcc and hcp hollow sites but did not lead to a clear discrimination between the onefold on-top and the sixfold coordinated substitutional site. This can be seen from Table I, where multiple minima are present for each site, none having a very low R factor. This is illustrated in Fig. 4 for the on-top site, where a three-dimensional plot is shown, from which the multiple minima can be seen, present for both variations of the K-Al and the Al-Al distances. It is to be noted that the smallest value of the R factor is still quite large ($R_{DE} \sim 0.6$).

Further refinement involving lateral and vertical relaxations of the substrate layers and variation of Θ_K did clearly indicate a preference for the on-top site, as is evident from Table II, in which the best-fit R factors for all sites considered are listed, together with the corresponding structural parameters. The energy step in the calculations was taken to be 5 eV, with eight beams, corresponding to 392 data points being used in the comparison between theory and experiment. (A calculation was also made for the determined on-top site with an energy step of 2.5 eV, 696 data points being used in the comparison between theory and experiment. The obtained R factors were very similar to those in Table II, i.e., 0.344, 0.310, and 0.110 for the R_{DE} and R_P and the R_{ZJ} factors, respectively.)

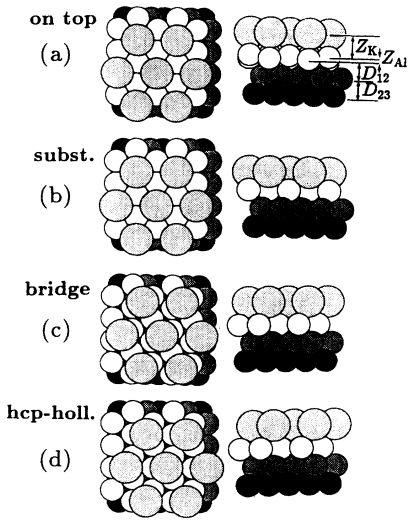

FIG. 3. The sites considered in the LEED analysis. In each case the large pale grey circles denote the K atoms, the white, dark grey, and black circles representing the first, second, and third Al layers, respectively. The ratio of the K radius to the Al radius corresponds to the covalent K radius and the hard core Al radius.

TABLE I. The minimum R_{DE} factors for each of the sites considered for the Al(111)-$(\sqrt{3}\times\sqrt{3})R30°$-K structure formed at 90 K on variation of Z_K and D_{12}. All other structural parameters are fixed at the ideal bulk values and Θ_K = 50 K, Θ_{Al} = 450 K. For each model V_o is optimized for best agreement with experiment.

R_{DE}	Z_K (Å)	D_{12} (Å)	Adsorption site
0.592	1.80	2.50	substitutional
0.585	2.26	2.51	substitutional
0.583	2.60	2.50	substitutional
0.568	3.00	2.50	substitutional
0.592	2.27	2.55	on-top
0.607	3.15	2.50	on-top
0.604	2.83	2.56	on-top
0.712	1.25	2.49	fcc hollow
0.657	2.30	2.52	fcc hollow
0.635	2.78	2.52	fcc hollow
0.623	3.22	2.49	fcc hollow
0.626	1.94	2.50	bridge
0.632	2.35	2.49	bridge
0.653	3.20	2.49	bridge
0.703	1.86	2.21	hcp hollow
0.674	2.31	2.25	hcp hollow
0.689	2.84	2.22	hcp hollow
0.719	3.20	2.19	hcp hollow

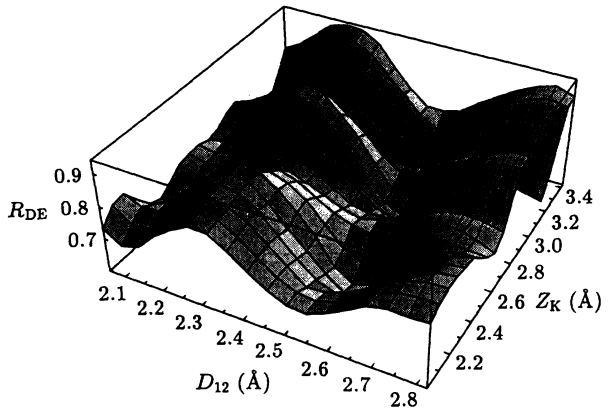

FIG. 4. Three-dimensional plot for the on-top adsorption geometry showing the R_{DE} factor as a function of the K-Al (Z_K) and first Al-Al (D_{12}) spacings.

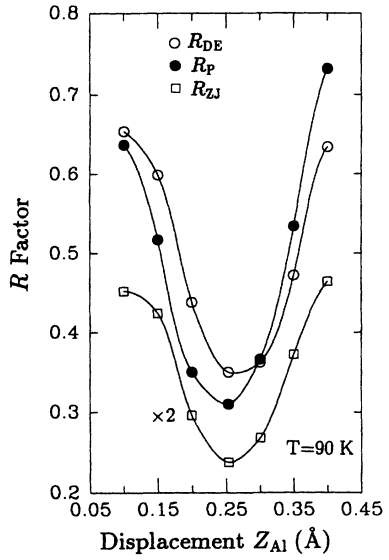

FIG. 5. Plot illustrating the R factor dependence for the on-top structure on Z_{Al} for the optimum K-Al spacing.

For the on-top site the best-fit structure, as sketched in Fig. 3(a), involves a rumpling of the first layer of Al atoms such that the Al atoms directly beneath the K atoms have moved in towards the bulk by 0.12 Å from the unrelaxed geometry and the other Al atoms in the first layer have moved outward by 0.13 Å from the unrelaxed geometry, giving rise to a vertical distance of 0.25 ± 0.04 Å between Al atoms in the first layer. The K atoms are found to be at a vertical distance of 2.98 ± 0.05 Å, from the uppermost Al atoms in the first layer giving a K-Al nearest-neighbor distance of 3.23 Å. Assuming a hard-sphere metallic radius of r_{Al} = 1.43 Å yields an effective K radius r_K = 1.80 Å. The vertical distances of the Al atoms in the uppermost Al layer, and the displaced Al atoms beneath the K atoms, to the second Al layer are found to be 2.46 Å and 2.21 ± 0.05 Å, respectively, as compared to the bulk interlayer spacing of 2.33 Å. The inward displacement of 1/3 of the Al atoms in the first layer was found to be accompanied by small outward lateral shifts of 0.05 Å of the nearest-neighbor Al atoms in the second layer. In particular, as can be seen from Fig. 5 the R factors are very sensitive to the displacement of the Al atom beneath the K atom where a deep, sharp minimum can be seen, corresponding to an improvement of the R_{DE} factor from ~ 0.6 to 0.350. In Fig. 6 the dependence of the R factors on Θ_K is shown. It can be seen that all R factors are also very sensitive to this value. From the analysis, values of V_o =6.0 ± 1.0 eV and Θ_K =110 ± 60 K were determined.

Using the obtained structural and nonstructural parameters described above, theoretical curves were obtained and are compared to the experimental results as shown in Fig. 7, from which good agreement is evident. A comparison of the experimental curves with the theoretical curves obtained for the most favorable geometry of the alternative sites is shown in Figs. 8(a)–8(d), where, as expected, the agreement is poor.

As mentioned earlier, calculations were performed using a different value of V_o for the K overlayer. In the calculation, refraction at the surface barrier is included but not reflection. From *ab initio* surface calculations,[11] as well as from surface band-structure calculations,[35] it follows that the interstitial potential in the K adlayer for the substitutional adsorption is between 2 and 3 eV higher (closer to the vacuum level) than it is in the Al substrate. As can be seen from Fig. 9, no improvement in the R factors is obtained for the on-top surface structure when this change of V_o is taken into account. For each (V_o^K, V_o^{Al}) combination, as shown in Fig. 9, an automatic structural refinement was carried out which led to very little change in the R factors and structural parameters.

C. The $(\sqrt{3} \times \sqrt{3})R30°$ structure: Room temperature

Following the same initial procedure as for the low-temperature results as described above (that is, optimiza-

TABLE II. The best-fit R factors for each of the sites considered for the Al(111)-$(\sqrt{3}\times\sqrt{3})R30°$-K structure formed at 90 K.

R_{DE}	R_{ZJ}	R_P	Z_K (Å)	D_{12} (Å)	D_{23} (Å)	Z_{Al} (Å)	Adsorption site
0.572	0.259	0.695	2.60	2.53	2.36		substitutional
0.365	0.137	0.335	2.98	2.21	2.33	0.25	on-top
0.318	0.101	0.287					top-split
0.655	0.327	0.797	2.78	2.52	2.33		fcc hollow
0.607	0.220	0.705	1.94	2.50	2.33		bridge
0.738	0.328	0.904	2.31	2.25	2.33		hcp hollow

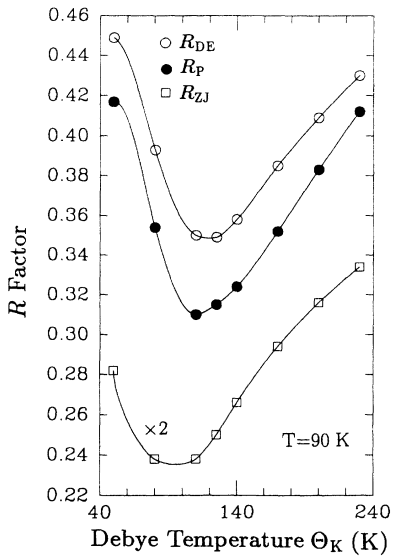

FIG. 6. Plot showing the variation of the R factors with Θ_K for the determined on-top site structure.

tion of the K-Al and Al-Al interlayer distances together with V_o with an energy step of 10 eV), it was found that the structure formed at 300 K showed a clear preference for the substitutional site. This can be seen from Table III, which shows the R factors and structural parameters for each site tested. For the substitutional site

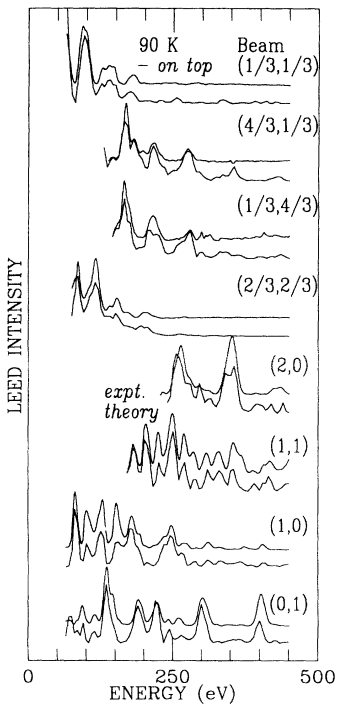

FIG. 7. Experimental and calculated intensity versus energy curves for the structure formed at 90 K. For each beam the experimental intensities are the upper curves. The calculated intensities are for the best-fit geometry for the on-top site, given in Table II and shown in Fig. 3(a).

Fig. 10 illustrates the R_{DE} factor in a three-dimensional plot, where it can be seen clearly that two minima are present; one is, however, deeper than the other. Further refinement involving lateral and vertical relaxations of the substrate and optimization of Θ_K enhanced the preference for the substitutional site. The best-fit R factors and corresponding structural parameters for the five sites considered are listed in Table IV, from which the preference for the substitutional site is again evident. A sketch of the structure is shown in Fig. 3(b), where the K atoms are in quasisubstitutional sites formed by the ejection of 1/3 of a monolayer of Al atoms. The K atoms are situated at a vertical distance of 2.16 ± 0.03 Å above the first layer of Al atoms, corresponding to a nearest-neighbor K-Al distance of 3.58 Å. Assuming a hard-sphere metallic radius $r_{Al} = 1.43$ Å yields an effective radius $r_K = 2.15$ Å, lying between the covalent radius of 2.03 Å and the metallic radius of 2.27 Å. The first Al interlayer spacing is contracted by 2 ±1 % with respect to the bulk value, whereas the second Al interlayer spacing is equal to the bulk value within the error of the determination. Figure 11 shows a plot of the R factors versus Θ_K, where it can be seen again that a sensitive variation is exhibited by each of the R factors. Optimum values of V_o =4.0 ± 1.0 eV and Θ_K =140 ± 50 K were determined in the analysis. A comparison of the experimental intensity curves with those calculated for the optimum geometry are shown in Fig. 12, from which very good agreement is observed. A comparison of the experimental curves with the theoretical curves obtained for the most favorable geometry of the alternative sites are shown in Figs. 13(a)–13(d), where the agreement is poor in each case. In the analysis, for the substitutional site, the positions of the displaced Al atoms were neglected. In view of the good agreement noted above, it seems unlikely that they form an ordered sublattice; rather, they are most probably readsorbed at steps. Calculations were also made for the case where the ejected Al atoms may reside in hollow sites above the potassium atoms, but an R factor analysis showed that this geometry was clearly unfavorable.

As for the analysis for the low-temperature structure, calculations were also made for different combinations of the inner potential for K (V_o^K) and Al (V_o^{Al}), as described in the previous section. The results are shown in Fig. 14. It can be seen that for the R_{DE} factor no improvement is obtained by taking a different inner potential for the K layer; the R_P factor, however, does show a slight improvement (from $R_P = 0.247$ to 0.242), for the combination (2,4) (i.e., the inner potential being 2 eV and 4 eV in the K layer and in the Al layers, respectively). It is to be noted that although the improvement is very slight, it can be seen from Fig. 9 for the on-top site that no improvement at all in the R factors was obtained.

It is interesting to note the differences in the inner potentials obtained for the clean surface and the alkali covered surfaces as given above in Secs. IV A, IV B, and IV C, the differences being none for the on-top site and 2.0 eV for the substitutional site. This is somewhat surprising, since first, a decrease is expected with alkali-metal adsorption as it reflects the decrease in the

work function, and second, the difference of 2.0 eV between the on-top value and the substitutional value is quite large given the coverage is the same. Therefore, some effort was made to obtain an accurate as possible value for the inner potential in each case. The refined values were 6.4 eV, 5.7 eV, and 3.6 eV for the clean, on-top, and substitutional structures, which, as it turns out, are not significantly different from the original values. The difference of approximately 2.0 eV between the on-top and substitutional geometries remains. Work function measurements of K/Al(111) have been performed by Horn *et al.*[36] at low temperature, where at cover-

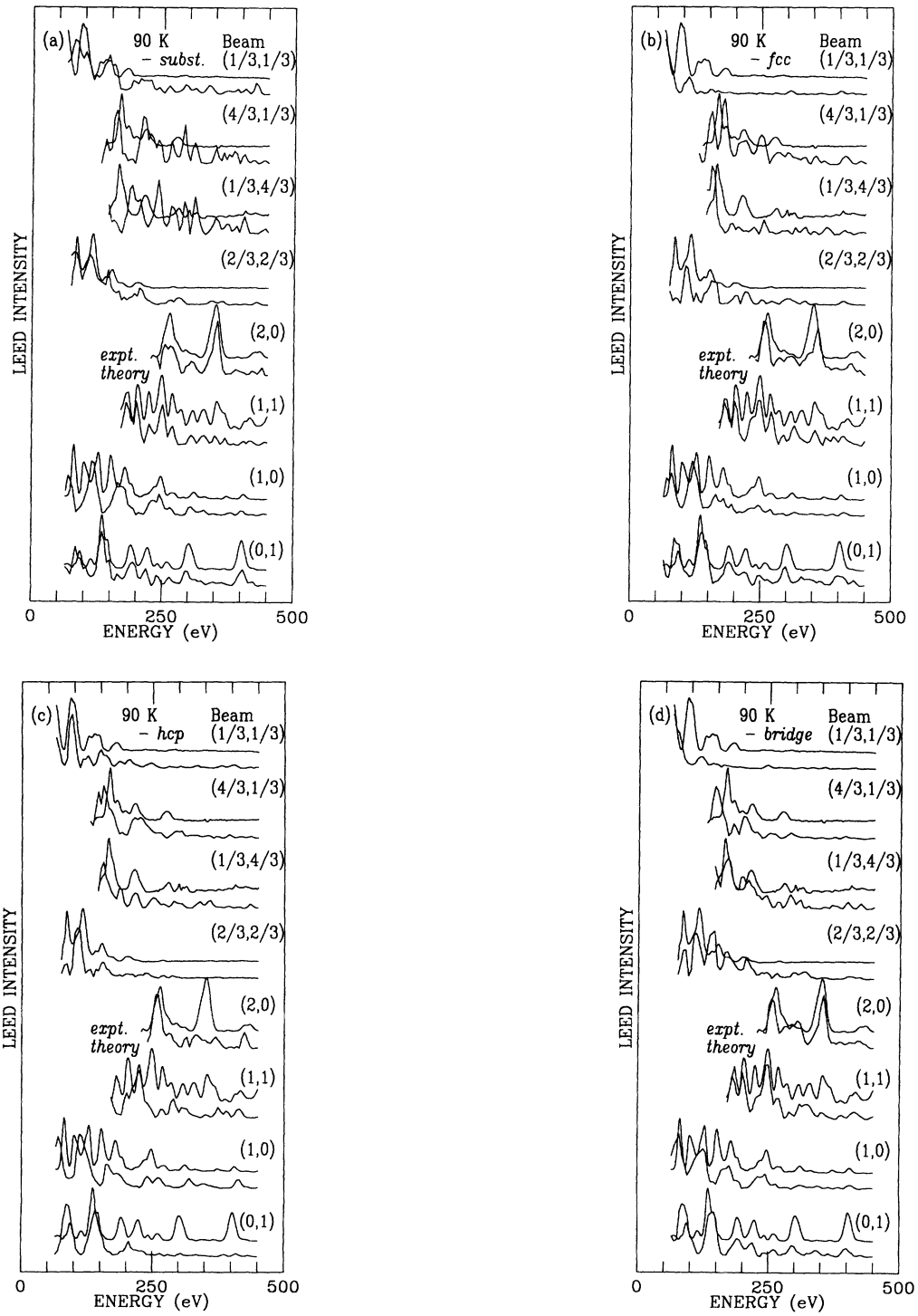

FIG. 8. Plots showing the comparison of the experimental intensity versus energy curves at low temperature with the calculated curves obtained using the best-fit geometry of the other sites considered; (a) substitutional (b) fcc hollow, (c) hcp hollow, and (d) bridge sites.

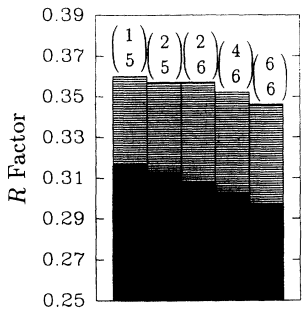

FIG. 9. Histogram showing the R factors for the obtained on-top structural geometry at low temperature for various values of V_o^K and V_o^{Al}. The dark shaded bars correspond to R_P while the lighter bars denote R_{DE} values.

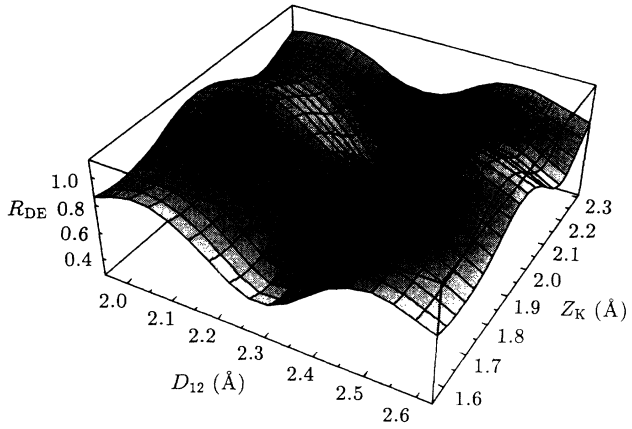

FIG. 10. Three-dimensional plot for the substitutional geometry showing the R_{DE} factor as a function of the K-Al spacing (Z_K) and the first Al-Al interlayer spacing (D_{12}).

age $\Theta = 1/3$ a decrease in the work function of approximately 1.9 eV is reported. From density-functional-theory (DFT) calculations,[37] a decrease in the work function of approximately 1.7 eV is obtained for both non-activated and activated adsorption (corresponding to the on-top and substitutional structures, respectively).

V. ANISOTROPIC EFFECTS

As shown by Over, Moritz, and Ertl,[21] it is possible, using LEED, to gain certain information about the dynamics of the system under investigation by introducing the concept of split position. In their work the $(\sqrt{3} \times \sqrt{3})R30°$-CO/Ru(0001) system was investigated, where it was found that the agreement between experimental and theoretical $I(E)$ curves could be significantly improved by including anisotropic vibrations. The idea of split position is that the probability-density function describing the thermal vibrations can be approximated using a few distinct positions with an appropriate occupation factor. The LEED calculation is then carried out for this geometry where all multiple scattering paths between the split positions are suppressed.

Anisotropic temperature effects were investigated for both the on-top site and the substitutional site. A split position of K used in the present calculations is illustrated in Fig. 15(a), where, in this case, the K positions are compatible with the threefold symmetry. In the calculation, the bond length obtained without using split positions was conserved. That is, the height of the K atom above the Al atom was accordingly reduced as the lateral distance from the exact on-top position was increased. Calculations were also made without reducing the height; similar results were obtained but the improvement in the R factors was not as great. By varying the split position (the lateral displacement) for a range of Θ_K (50, 100, 150, 200, and 250 K) it was found that for the on-top site the R factors were significantly improved, the K atom exhibiting an average lateral displacement of approximately 0.30 Å from the exact on-top position for $\Theta_K = 150$ K. It can be seen from Fig. 16(a) that the minima of the three R factors occur at slightly different split position values. For the R_{DE} factor the minimum occurs at 0.30 Å, for the R_P factor at 0.35 Å, and for the R_{ZJ} factor at 0.375 Å. (We choose to quote 0.30 Å, since the R_{DE} factor is sensitive to relative intensities which vibrational amplitudes affect more.) The R factors obtained were reduced from 0.365, 0.335, and 0.137 to 0.318, 0.287, and 0.101 for the R_{DE}, R_P and R_{ZJ} factors, respectively. In general, for the range of Θ_K and split positions tested, on the criteria of best R factor, an increase in Debye temperature occurs as the split position distance is increased. This increase is expected because the thermal vibrations, in part, have, with the use of split positions, been taken into account (a large Debye temperature indicates a smaller vibrational amplitude). The remaining vibrations not included in the description provided by split positions are taken into account by the Debye-Waller factor using the Debye temperature. This is schematically shown in Figs. 15(b) and 15(c), which illustrate the description of thermal vibrations within the Debye model (with $\Theta_K = 110$K) and when using split positions (with $\Theta_K = 150$ K), respectively. The root mean square displacements corresponding to the Debye temperatures of 110 and 150 K are $\langle u^2 \rangle^{1/2} \simeq 0.15$ Å and

TABLE III. The minimum R_{DE} factors for each of the sites considered for the Al(111)-$(\sqrt{3}\times\sqrt{3})R30°$-K structure formed at 300 K on variation of Z_K and D_{12}. All other structural parameters are fixed at the ideal bulk values and $\Theta_K = 50$ K, $\Theta_{Al} = 450$ K. For each model V_o is optimized for best agreement with experiment.

R_{DE}	Z_K (Å)	D_{12} (Å)	Adsorption site
0.479	1.70	2.28	substitutional
0.449	2.15	2.27	substitutional
0.564	2.15	2.30	on-top
0.598	2.63	2.29	on-top
0.553	1.37	2.31	fcc hollow
0.554	1.87	2.29	fcc hollow
0.536	2.38	2.29	bridge
0.538	2.83	2.29	bridge
0.835	1.37	2.13	hcp hollow
0.808	1.85	2.07	hcp hollow

TABLE IV. The best fit R factors for each of the sites considered for the Al(111)-($\sqrt{3} \times \sqrt{3}$)$R30°$-K structure formed at 300 K.

R_{DE}	R_{ZJ}	R_P	Z_K(Å)	D_{12}(Å)	D_{23}(Å)	Z_{Al}(Å)	Adsorption site
0.284	0.126	0.280	2.16	2.29	2.34		substitutional
0.536	0.213	0.714	2.15	2.20	2.32	0.15	on-top
0.590	0.342	0.705	1.87	2.29	2.34		fcc hollow
0.554	0.240	0.686	2.38	2.29	2.34		bridge
0.863	0.353	0.949	1.85	2.07	2.34		hcp hollow

0.10 Å, respectively. The thermal motion described by the split position is much larger than the isotropic motion within the Debye model. Using the simple model of a two-dimensional quantum mechanical harmonic oscillator, the excitation energy of the lateral vibrational mode is estimated to be approximately 3 meV.[38] These results are similar to those obtained by Over *et al.*[39] for the Cs/Ru(0001) system in that the R factors were significantly reduced for the (2 × 2) on-top structure but not for the ($\sqrt{3} \times \sqrt{3}$)$R30°$ hcp structure. In this case a value of 1 meV for the excitation energy of the lateral vibrational mode was obtained.

To best see the effect on the intensities of the inclusion of anisotropic temperature effects using split positions, a comparision of the theoretical intensities with and without using split positions is shown in Fig. 17. The lateral displacement was 0.30 Å. It can quickly be seen that the main difference lies in the fractional-order beams, in particular for the higher order fractional-order beams [beams (4/3,1/3) and (1/3,4/3)]. An automatic refinement was carried out to see whether this description of the temperature effects led to any change in the previous structural determination. The structure was found to be unchanged. Various other azimuthal orientations of the displacements were also considered with three positions. Further, not just three but six equivalent positions were considered. As in Ref. 21, no significant differences for the mentioned geometries were found; this can be rationalized by the consideration that the same interatomic vectors in the overlayer occur with three sites as well as with six sites when the vectors between split positions are ignored.

For the substitutional site, no significant improvement in the R factors was found [see Fig. 16(b)]. These findings seem reasonable in that the K atom sits lower in the substitutional site and is sixfold coordinated, both factors reducing the possibility of movement; further, the K atom is in the stable adsorption site.

VI. DISCUSSION

The results of the present LEED analysis can be compared to DFT calculations by Neugebauer and Scheffler[11]

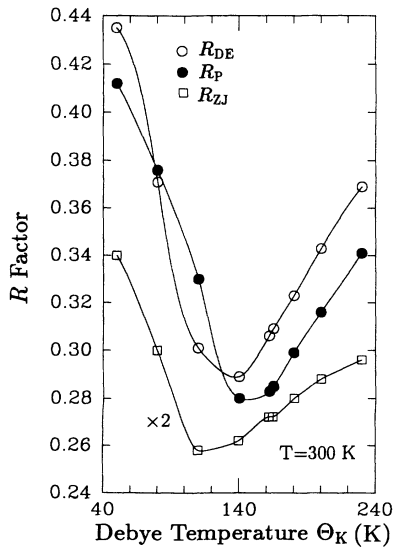

FIG. 11. Plot showing the variation of the R factors with Θ_K for the determined substitutional site geometry.

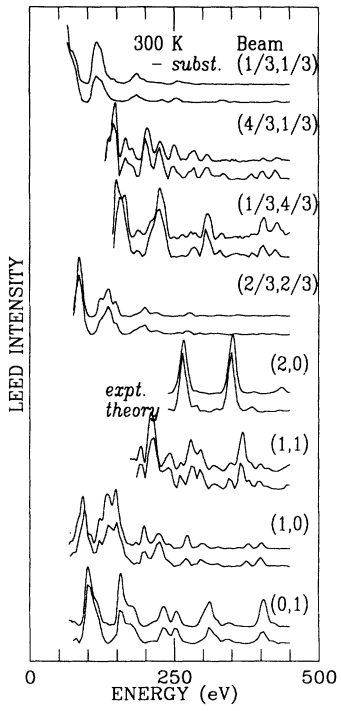

FIG. 12. Experimental and calculated intensity versus energy curves for the structure formed at 300 K. For each beam the experimental intensities are the upper curves. The calculated intensities are for the best-fit geometry for the substitutional site, given in Table IV and as shown in Fig. 3(b).

for the adsorption of K on Al(111). These calculations show that the adsorption energies for occupation of on-top, fcc-hollow, and substitutional sites are almost degenerate, having adsorption energies of 1.21, 1.20, and 1.17 eV, respectively. Furthermore, they showed that the vacancy-formation energy is particularly small (0.41 eV). This, together with the result obtained by Stumpf and Scheffler[40] that an Al adsorbate on an Al(111) surface has a very high diffusivity, is consistent with substitutional site occupation where the ejected Al atom moves to a step or kink—and indeed there are steps, at least on the Na/Al(111) surface, as has been shown by scanning-

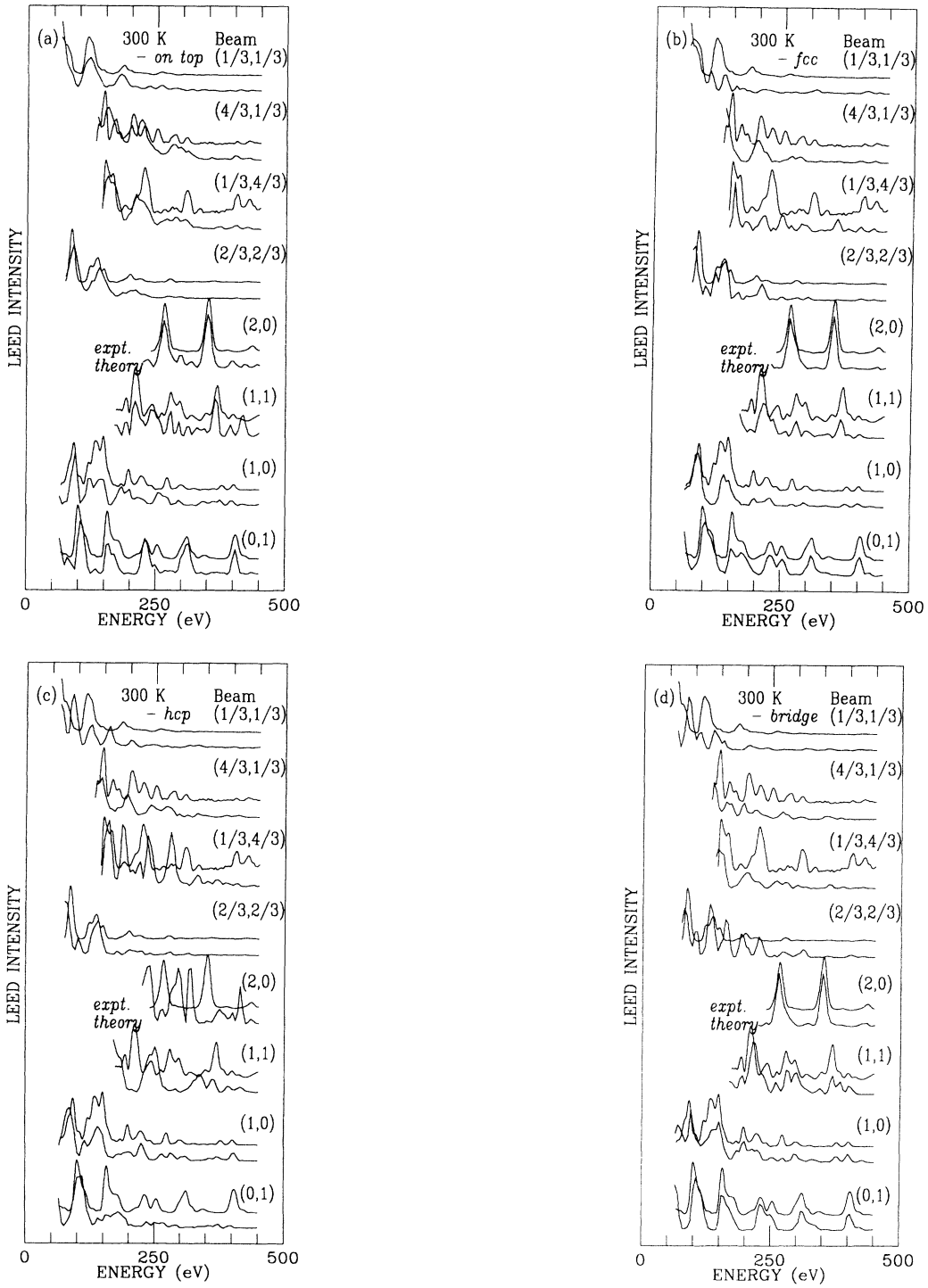

FIG. 13. Plots showing the comparison of the experimental intensity versus energy curves for the room-temperature structure with the calculated curves obtained using the best-fit geometries of the other sites; (a) on-top (b) fcc hollow, (c) hcp hollow, and (d) bridge sites.

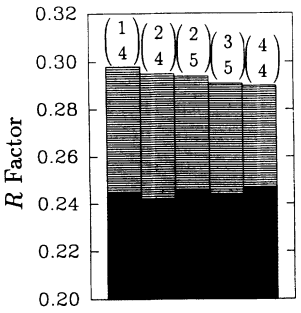

FIG. 14. Histogram showing the R factors for the determined substitutional structural geometry for various values of V_o^K and V_o^{Al}. The dark shaded bars correspond to R_P while the lighter bars denote R_{DE} values.

tunneling-microscopy investigation.[41]

The values obtained by the DFT calculations for the bond lengths of the $(\sqrt{3} \times \sqrt{3})R30°$ structures are 3.70 and 3.38 Å for the substitutional and on-top sites, respectively. These values are in reasonable agreement with the values determined by the present LEED analysis of 3.58 and 3.23 Å. The change in bond length between the onefold on-top site and the sixfold substitutional site obtained from the DFT calculations is 0.32 Å, which agrees very well with the present result of 0.35 Å. The DFT calculations agree much better with the present result than the value of 0.5 Å obtained using an empirical relationship given by Kittel,[42] which assumes the nature of bonding is the same for each structure. An increase in bond length with adatom coordination reflects the idea that the bonding saturates; thus the bond strength per bond decreases. The bond length and adatom coordi-

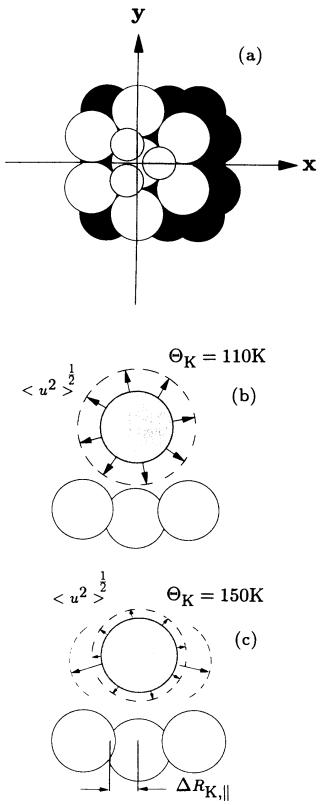

FIG. 15. (a) An illustration of a split position for K in the on-top position. Here the K atoms possess threefold symmetry and are represented by the smaller pale grey circles. It is to be noted that for clarity, the ratio of the K radius to the hard core Al radius is shown as being approximately 50% smaller than that if the covalent K radius is used, and also the magnitude of the split position is exaggerated. On-top site: (b) schematic diagram illustrating the description of thermal vibrations using the Debye model and (c) using split positions, indicating the increase of Θ_K and corresponding decrease in the root mean square displacement of the adatom from its mean position u when split positions are used.

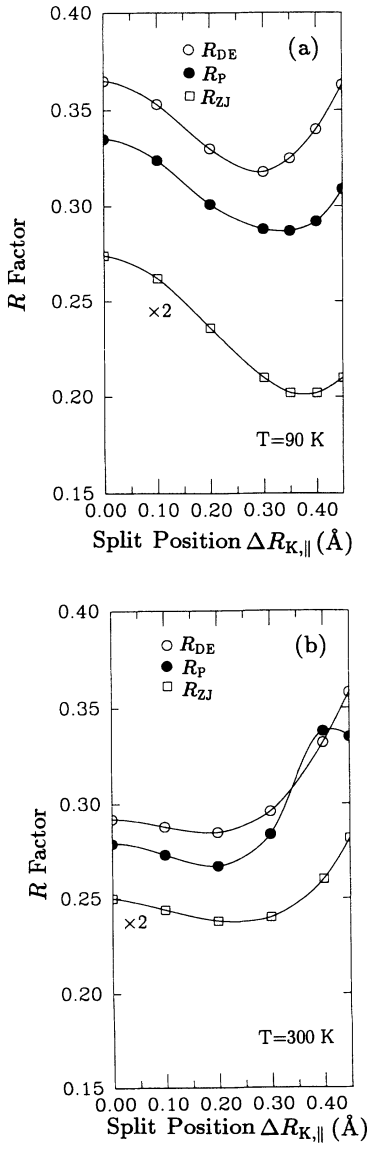

FIG. 16. Plot of the R factors obtained using the split position concept to describe anisotropic temperature effects; (a) on-top site, (b) substitutional site.

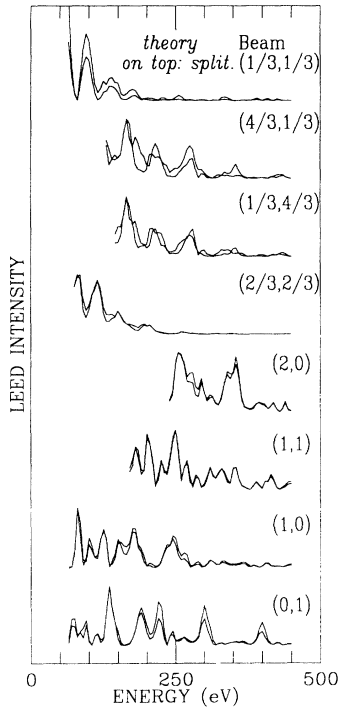

FIG. 17. Plot showing the effect on the intensities of the inclusion of anisotropic temperature effects where the theoretical intensities obtained with and without using the split position (0.30 Å) for Θ_K=150 K are compared.

nation number of other quantitatively determined structures of different alkali-metal/metal adsorption systems (e.g., see Table I of Ref. 43) can be compared.

The present results give a first indication of the nature of the phase transition and the mechanism for the ejection of Al atoms necessary to form the substitutional adsorption. We find that on-top adsorption is metastable for the $(\sqrt{3} \times \sqrt{3})R30°$ structure. Thus, for the *periodic* layer a structural phase transition to substitutional adsorption becomes possible, having the most favorable free energy. Our results indicate that warming to 300 K is sufficient to overcome the activation barrier for this transition. By *guessing a particular reaction path*, DFT calculations indicate a value for the activation barrier. If the path is such that the ejected substrate atom moves to a step and is rebonded there, the activation barrier from the on-surface adatom to the surface substitutional is 0.8 eV; namely, the energy of an on-surface adatom minus the energy of the substitutional adatom plus an adsorbed Al atom. Alternatively, this energy barrier can be considered to be the energy difference between the creation of a "distant Frenkel pair" consisting of the vacancy and an Al atom somewhere on the surface nearby and that of creating a vacancy where the ejected Al atom resides at a step. By simple considerations this value can be used to obtain some insight into the dependence on the temperature of the transition. The Arrhenius equation below relates the rate of the transition r with the activation barrier and temperature,

$$r = 1/\nu \times \exp(-E^b/k_B T), \quad (1)$$

where ν is the time of a single vibration and is typically in the range 10^{-11}–10^{-13} s. $1/\nu$ can be thought of as the attempt frequency of the atom to overcome the barrier. T is the temperature, k_B the Boltzmans constant, and E^b is the activation barrier height. It is to be noted that the present on-top–to–substitutional transition is more complex than, for example, an on-top–to–bridge transition because it involves the ejected Al atom. With the latter type of transition Eq. (1) is applicable; however, to apply Eq. (1) to the former transition, it should be assumed either that the transition occurs near a step or kink, as in that case the excursion of the ejected Al atom to the step or kink can be neglected, or alternatively that the place exchange is rate determining, i.e., much slower than diffusion of an Al atom to a step [this is indeed true; compare 0.8 eV to the diffusion barrier, 0.04 eV, of an Al adatom on an Al(111) surface.[40]] From Eq. (1) it can be seen that the value of 0.8 eV for the activation barrier, as shown schematically in Fig. 18(a), is in accord with the experimental analysis because a barrier of 0.8 eV implies that the transition could occur with measurable rate at temperatures of the order of 240 ±20 K but with negligi-

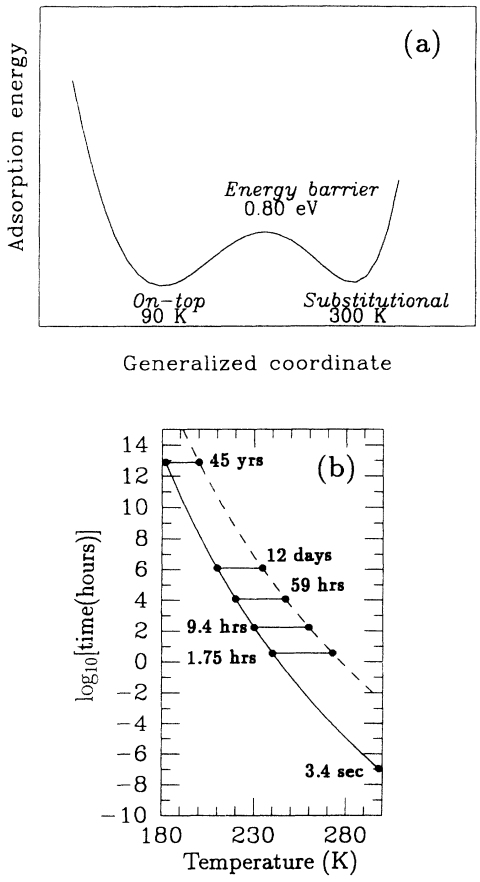

FIG. 18. (a) Schematic diagram illustrating the energy barrier that exists between the on-top site at low temperature and the substitutional site at room temperature. (b) Plot of the time (on a logarithmic scale) to form the substitutional potassium overlayer versus temperature, obtained using Eq. (1).

ble rate at 180 K for example. Fig. 18(b) illustrates this, where the time to form the $(\sqrt{3} \times \sqrt{3})R30\,°$K substitutional structure is plotted (on a logarithmic scale) against temperature, taking $\nu = 10^{-13}$ s (continuous line) and $\nu = 10^{-11}$ s (dashed line).

VII. CONCLUSION

A LEED structural analysis of the $(\sqrt{3}\times\sqrt{3})R30°$ system formed by adsorption of K on Al(111) at two different temperatures (90 K and 300 K) shows that the two conditions give rise to the same periodicity but a significantly different local geometry and bonding nature. The structure formed at 90 K contains K atoms in on-top sites on a rumpled first layer of Al atoms. This structure is metastable and converts to a structure containing K atoms in a sixfold coordinated substitutional site on warming to 300 K, the substitutional site being favorable due to the low vacancy formation energy for a $(\sqrt{3}\times\sqrt{3})R30°$ vacancy surface structure and a reduced alkali-alkali repulsion.[11] Furthermore, using the method of split positions to take into account anisotropic temperature effects, information about the dynamics of the K atom was able to be determined, in that for the on-top adsorption site the K atom vibrates predominantly laterally with an associated split position of approximately 0.30 Å. No such effect was exhibited for the stable substitutional site at room temperature, which can be understood in that the potassium atom is "locked in."

ACKNOWLEDGMENTS

The authors wish to acknowledge useful discussions with Jesper Andersen, Jochen Haase, Jörg Neugebauer, Renee Diehl, and Martin Gierer. Support of this work by the Danish Natural Science Research Council and Center for Surface Reactivity is gratefully acknowledged. H. O. acknowledges financial support from the Deutsche Forschungsgemeinschaft.

* Present address: Department of Physics and Laboratory for Surface Studies, University of Wisconsin-Milwaukee, Milwaukee, Wisconsin 53201.

[1] For a recent review, see N. D. Lang, in *Physics and Chemistry of Alkali Metal Adsorption*, edited by H. P. Bonzel, A. M. Bradshaw, and G. Ertl (Elsevier, Amsterdam, 1989).
[2] S. Andersson and J. Pendry, Solid State Commun. **16**, 563 (1975).
[3] J. Demuth, D. Jepsen, and P. Marcus, J. Phys. C **8**, L25 (1975).
[4] B. Hutchins, T. Rhodin, and J. Demuth, Surf. Sci. **54**, 419 (1976).
[5] S. Lindgren, L. Walldén, J. Rundgren, P. Westrin, and J. Neve, Phys. Rev. B **28**, 6707 (1983).
[6] H. Over, H. Bludau, M. Skottke-Klein, G. Ertl, W. Moritz, and C. Campbell, Phys. Rev. B **45**, 8638 (1992).
[7] M. Kerkar, D. Fisher, D. P. Woodruff, R. Jones, R. Diehl, C. McConville, and B. Cowie, J. Vac. Sci. Technol. A **10**, 2148 (1992).
[8] D. Fisher, S. Chandavarkar, I. R. Collins, R. Diehl, P. Kaukasoina, and M. Lindroos, Phys. Rev. Lett. **68**, 2786 (1992).
[9] A. Schmalz, S. Aminpirooz, L. Becker, J. Haase, J.Neugebauer, M. Scheffler, D. R. Batchelor, D. L. Adams, and E. Bøgh, Phys. Rev. Lett. **67**, 2163 (1991).
[10] M. Gierer, H. Bludau, T. Hertel, H. Over, W. Moritz, and G. Ertl, Surf. Sci. Lett. **279**, L170 (1992).
[11] J. Neugebauer and M. Scheffler, Phys. Rev. B **46**, 16 067 (1992).
[12] C. Stampfl, M. Scheffler, H. Over, J. Burchhardt, M. Nielsen, D. L. Adams and W. Moritz, Phys. Rev. Lett. **69**, 1532 (1992).
[13] J. N. Andersen, E. Lundgren, R. Nyholm, and M. Qvarford, Phys. Rev. B **46**, 12 784 (1992).
[14] S. Aminpirooz, A. Schmalz, N. Pangher, J. Haase, M. M. Nielsen, D. R. Batchelor, E. Bøgh, and D. L. Adams, Phys. Rev. B **46**, 15 594 (1992).
[15] J. N. Andersen, E. Lundgren, R. Nyholm and M. Qvarford, Surf. Sci. **289**, 307 (1993).
[16] M. Kerkar, D. Fisher, D. P. Woodruff, R. G. Jones, R. D. Diehl, and B. Cowie, Surf. Sci. **278**, 246 (1992).
[17] T. Aruga, H. Tochihara, and Y. Murata, Surf. Sci. **175**, L725 (1986).
[18] S. Modesti, C. T. Chen, Y. Ma, G. Meigs, P. Rudolf and F. Sette, Phys. Rev. B **42**, 5381 (1990).
[19] G. M. Lamble, R. A. Brooks, D. A. King, and D. Norman, Phys. Rev. Lett. **61**, 1112 (1988).
[20] R. J. Behm, in *Physics and Chemistry of Alkali Metal Adsorption*, edited by H. P. Bonzel, A. M. Bradshaw, and G. Ertl (Elsevier, Amsterdam, 1989).
[21] H. Over, W. Moritz, and G. Ertl, Phys. Rev. Lett. **70**, 315 (1993).
[22] H. W. Jørgensen, Ph.D. thesis, Aarhus University, 1976.
[23] SAES Getters Spa, Milano, Italy.
[24] D. L. Adams, S. P. Andersen, and J. Burchhardt, in *The Structure of Surfaces III*, edited by S. Y. Tong, M. A. Van Hove, X. Xide, and K. Takayanagi (Springer, Berlin, 1991).
[25] M. M. Nielsen, J. Burchhardt, and D. L. Adams (unpublished).
[26] W. Moritz, J. Phys. C **17**, 353 (1983).
[27] H. Over, U. Ketterl, W. Moritz, and G. Ertl, Phys. Rev. B **46**, 15 438 (1992).
[28] J. B. Pendry, *Low Energy Electron Diffraction* (Academic Press, London 1974).
[29] G. Kleinle, W. Moritz, and G. Ertl, Surf. Sci. **238**, 119 (1990); G. Kleinle, W. Moritz, D. L. Adams, and G. Ertl, *ibid.* **219**, L637 (1989).
[30] V. Moruzzi, J. Janak, and A. Williams, *Calculated Electronic Properties of Metals* (Pergamon, New York, 1978).
[31] H. B. Nielsen and D. L. Adams, J. Phys. C **15**, 615 (1982).
[32] J. R. Noonan and H. L. Davis, J. Vac. Sci. Technol. A **8**, 2671 (1990).
[33] J. B. Pendry, J. Phys. C **13**, 937 (1980).
[34] E. Zanazzi and F. Jona, Surf. Sci. **62**, 61 (1977).

[35] B. Wenzien, J. Bormet, J. Neugebauer, and M. Scheffler, Surf. Sci. **287/288**, 559 (1993).
[36] K. Horn, A. Hohlfeld, J. Somers, Th. Lindner, P. Hollins and A. M. Bradshaw, Phys. Rev. Lett. **61**, 2488 (1988); A. Hohlfeld and K. Horn, Surf. Sci. **211/212**, 844 (1989).
[37] J. Neugebauer and M. Scheffler, Phys. Rev. Lett. **71**, 577 (1993).
[38] C. Cohen-Tannoudji, B. Diu, and F. Laloë, *Quantum Mechanics* (John Wiley and Sons, New York, 1977), Vol. 1; see also Ref. 28, p. 193.
[39] H. Over, M. Gierer, T. Hertel, H. Bludau, and G. Ertl (unpublished).
[40] R. Stumpf and M. Scheffler, Phys. Rev. Lett. (to be published).
[41] H. Brune, Ph.D. thesis, Frei Universität Berlin, 1992.
[42] C. Kittel, *Introduction to Solid State Physics*, (J. Wiley and Sons Inc., New York, 1986), p. 77.
[43] C. Stampfl, J. Burchhardt, M. Nielsen, D. L. Adams, M. Scheffler, H. Over, and W. Moritz, Surf. Sci. **287/288**, 418 (1993).

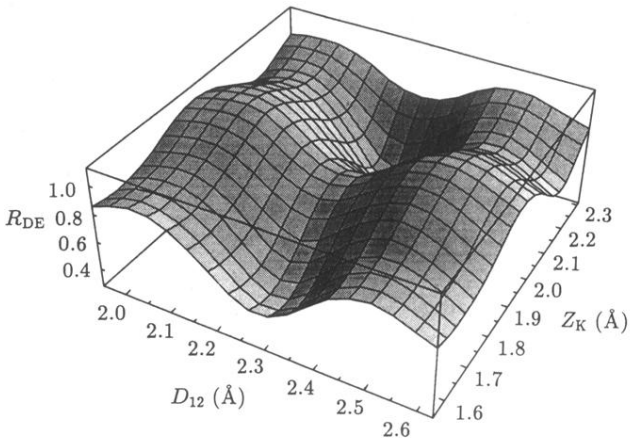

FIG. 10. Three-dimensional plot for the substitutional geometry showing the R_{DE} factor as a function of the K-Al spacing (Z_K) and the first Al-Al interlayer spacing (D_{12}).

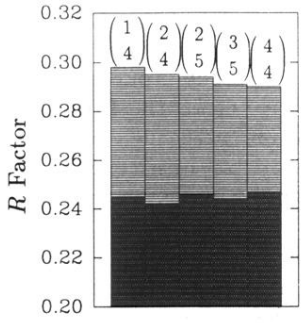

FIG. 14. Histogram showing the R factors for the determined substitutional structural geometry for various values of V_o^K and V_o^{Al}. The dark shaded bars correspond to R_P while the lighter bars denote R_{DE} values.

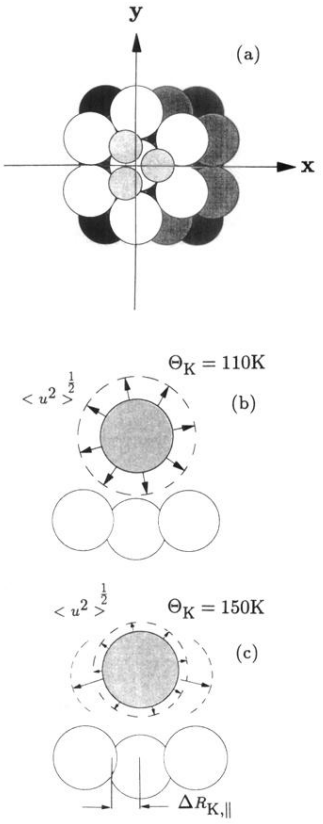

FIG. 15. (a) An illustration of a split position for K in the on-top position. Here the K atoms possess threefold symmetry and are represented by the smaller pale grey circles. It is to be noted that for clarity, the ratio of the K radius to the hard core Al radius is shown as being approximately 50% smaller than that if the covalent K radius is used, and also the magnitude of the split position is exaggerated. On-top site: (b) schematic diagram illustrating the description of thermal vibrations using the Debye model and (c) using split positions, indicating the increase of Θ_K and corresponding decrease in the root mean square displacement of the adatom from its mean position $\underline{u}$ when split positions are used.

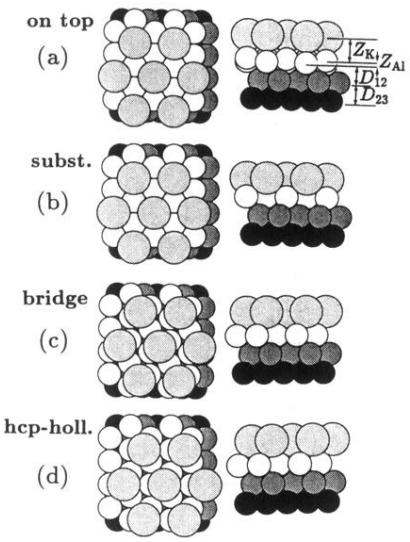

FIG. 3. The sites considered in the LEED analysis. In each case the large pale grey circles denote the K atoms, the white, dark grey, and black circles representing the first, second, and third Al layers, respectively. The ratio of the K radius to the Al radius corresponds to the covalent K radius and the hard core Al radius.

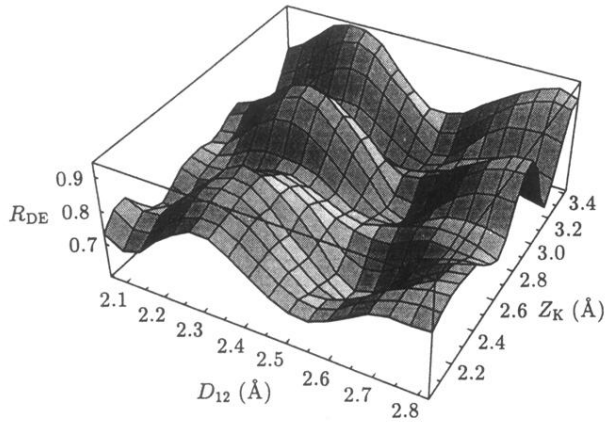

FIG. 4. Three-dimensional plot for the on-top adsorption geometry showing the R_{DE} factor as a function of the K-Al (Z_K) and first Al-Al (D_{12}) spacings.

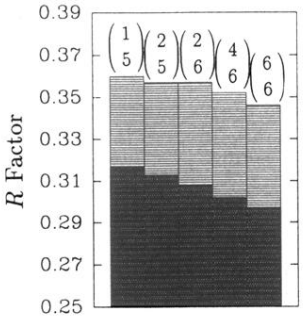

FIG. 9. Histogram showing the R factors for the obtained on-top structural geometry at low temperature for various values of V_o^K and V_o^{Al}. The dark shaded bars correspond to R_P while the lighter bars denote R_{DE} values.